PAPER

Improvement of signal-to-interference ratio and signal-to-noise ratio in nerve cuff electrode systems

IOP PUBLISHING PHYSIOLOGICAL MEASUREMENT

Physiol. Meas. **33** (2012) 943–967 doi:10.1088/0967-3334/33/6/943

Improvement of signal-to-interference ratio and signal-to-noise ratio in nerve cuff electrode systems

Jun-Uk Chu[1,4], Kang-Il Song[1,2,4], Sungmin Han[1], Soo Hyun Lee[3], Jinseok Kim[1], Ji Yoon Kang[3], Dosik Hwang[2], Jun-Kyo Francis Suh[1], Kuiwon Choi[1] and Inchan Youn[1,5]

[1] Biomedical Research Institute, Korea Institute of Science and Technology, 39-1, Hawolgok-dong, Seongbuk-gu, Seoul, 136-791, Korea
[2] School of Electrical and Electronic Engineering, Yonsei University, 134 Shinchon-dong, Seodaemun-gu, Seoul, 120-749, Korea
[3] Brain Science Institute, Korea Institute of Science and Technology, 39-1, Hawolgok-dong, Seongbuk-gu, Seoul, 136-791, Korea

E-mail: iyoun@kist.re.kr

Received 7 December 2011, accepted for publication 20 March 2012
Published 3 May 2012
Online at stacks.iop.org/PM/33/943

Abstract

Cuff electrodes are effective for chronic electroneurogram (ENG) recording while minimizing nerve damage. However, the ENG signals are usually contaminated by electromyogram (EMG) activity from the surrounding muscles, stimulus artifacts produced by the electrical stimulation and noise generated in the first stage of the neural signal amplifier. This paper proposed a new cuff electrode to reduce the interference from EMG signals and stimulus artifacts. As a result, when an additional middle electrode was placed at the center of the cuff electrode, a significant improvement in the signal-to-interference ratio was achieved at 11% for the EMG signals and 12% for the stimulus artifacts when compared to a conventional tripolar cuff. Furthermore, a new low-noise amplifier was proposed to improve the signal-to-noise ratio. The circuit was designed based on a noise analysis to minimize the noise, and the results show that the total noise of the amplifier was below 1 μV for a cuff impedance of 1 kΩ and a frequency bandwidth of 300 to 5000 Hz.

Keywords: cuff electrode, peripheral nerve, revised quasi-tripole configuration, low-noise amplifier

(Some figures may appear in colour only in the online journal)

[4] These authors contributed equally to this paper.
[5] Author to whom any correspondence should be addressed.

1. Introduction

Over the last few decades, cuff electrodes have been studied to facilitate neural recordings from peripheral nerves since they allow minimal invasive measurement and chronic implantation. The purpose of early studies was to explore the physiology of neuromuscular system while chronically implanting the cuff electrode as a tool to record peripheral nerve activity (reviewed by Struijk *et al* (1999)). Axonal conduction velocity was measured from the femoral nerve to access the order of motor neuron recruitment in walking cat (Hoffer *et al* 1987). Cutaneous afferent activity was recorded from the median nerve of a monkey to investigate the correlation with grip force during grasping and lifting (Milner *et al* 1991). Long-term effects of axotomy were studied following the change in cuff electrode recordings after peripheral nerves were cut and sutured to their distal end to permit regeneration (Davis *et al* 1978).

Such neural recordings can also provide useful information on specific targeted sensory or motor organs in spinal cord and brain injured human individuals, and realize feedback control for functional electrical stimulation (FES) systems (reviewed by Sinkjaer (2000) and Sinkjaer *et al* (2003)). To enhance the efficiency and reliability of FES systems, it is important to more accurately measure peripheral nerve activity as a feedback signal. Recently, attempts have been made to utilize cuff electrode recordings in various areas of clinical FES application. Hemiplegic subjects were implanted with a recording cuff electrode on the sural nerve to detect gait events for the correction of footdrop (Sinkjaer *et al* 1994, Haugland and Sinkjaer 1995, Hansen *et al* 2002, 2004). Sensory nerve signal was recorded from the volar nerve to the radial side of the index finger to detect the occurrence of slips in quadriplegic patients for hand grasp restoration (Haugland *et al* 1999). Afferent nerve activity from sacral root nerve was used to monitor intravesical pressure in spinal cord injured patients for bladder control (Kurstjens *et al* 2005).

In neural recording applications, a nerve cuff electrode system is generally comprised of a cuff electrode and neural signal amplifier. Figure 1 shows a conceptual block diagram of the entire nerve cuff electrode system. The cuff electrode is placed around the length of a peripheral nerve and picks up extracellular potentials that propagate along the axons in the nerve. The neural signal amplifier then selectively amplifies the electroneurogram (ENG) signals in an electrically noisy environment. The output of the neural signal amplifier is finally stored by a data acquisition system with display and analysis capabilities.

One of the important issues when designing a detection system for ENG signals is interference from external sources, including electromyogram (EMG) signals, electrical stimulation artifacts and power lines. Originally, a tripolar cuff electrode was proposed to reduce the influence of external sources, where three equally spaced ring electrodes are enclosed in an insulating cuff (Hoffer 1975, Stein *et al* 1975). The ENG signals are then detected differentially between the electrically shorted end electrodes and the middle electrode. This configuration is referred to as a *quasi-tripole* (QT) and has been widely used in ENG recordings (Pflaum *et al* 1996, Struijk and Thomsen 1995). The principle of the QT configuration is that the insulating cuff linearizes the internal field induced by external sources so that the resulting field is cancelled by the symmetrical placement of the electrodes. In practice, however, interference from external sources, such as EMG signals, is still present at the output of the neural signal amplifier since the tissue impedance inside the cuff is not uniform. To resolve this problem, different configurations have been proposed. For example, the *true-tripole* (TT) (Pflaum *et al* 1996), *screened-tripole* (ST) (Rahal *et al* 2000), and *adaptive-tripole* (AT) (Demosthenous *et al* 2004), all try to compensate for the cuff imbalance caused by cuff asymmetries and tissue growth, yet the increased circuit complexity and correspondingly high power consumption

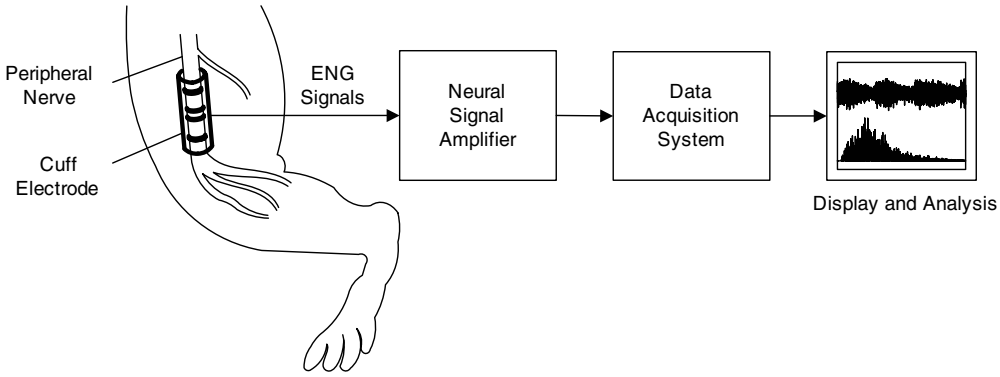

Figure 1. Block diagram of nerve cuff electrode system.

render these configurations less favorable for implantation. Consequently, a simple efficient configuration for a cuff electrode design is needed to enhance the signal-to-interference ratio (SIR).

Another important design issue is that ENG signals are easily contaminated with intrinsic system noise, including the thermal noise of the electrode–tissue interface impedance and voltage and current noise of the neural signal amplifier. From the viewpoint of noise analysis, the ENG signal source has source impedance (i.e. electrode–tissue interface impedance) that is related to a thermal noise generator. In addition, the neural signal amplifier itself has internal sources that act as a voltage noise generator and current noise generator. These two sources are known as electronic noise and mainly occur in the first stage of the neural signal amplifier. As a result, such thermal and electronic noises constitute the total noise that appears as the noise floor in ENG recordings. Furthermore, depending on the type of electrodes used, minimizing the electronic noise can be a critical factor when designing the neural signal amplifier. For example, when extracellular action potentials are measured with a needle-type microelectrode in a peripheral nerve, the source impedance is larger than 10 kΩ and the amplitudes of the recorded ENG signals are higher than 10 μV (Malagodi *et al* 1989). In this case, the total noise is essentially unaffected by the electronic noise of the preamplifier. That is, the contribution of the electronic noise is only a small fraction of the thermal noise. However, in the case of a cuff electrode, the source impedance is as small as 1 kΩ and the amplitudes of the recorded ENG signals are only on the order of a few microvolts. Since the ENG signals are now comparable to the noise floor, the contribution of the electronic noise cannot be neglected. Consequently, an optimized low-noise preamplifier design is needed for cuff electrodes to increase the signal-to-noise ratio (SNR).

Accordingly, the current study presents a new design for a nerve cuff electrode system to improve the SIR and SNR for measuring nerve signals. It was found that a *revised quasi-tripole* (rQT) configuration could reduce the interferences from EMG signals and stimulus artifacts more efficiently than a conventional QT configuration. In addition, the noise from the preamplifier could be minimized with a signal amplifier design based on an equivalent noise model. The electrical performance of the proposed cuff electrode system was evaluated using an *in vitro* model, and then applied to a rat animal model to record the ENG signals from the sciatic nerve during mechanical stimuli as well as electrical stimuli under anesthesia.

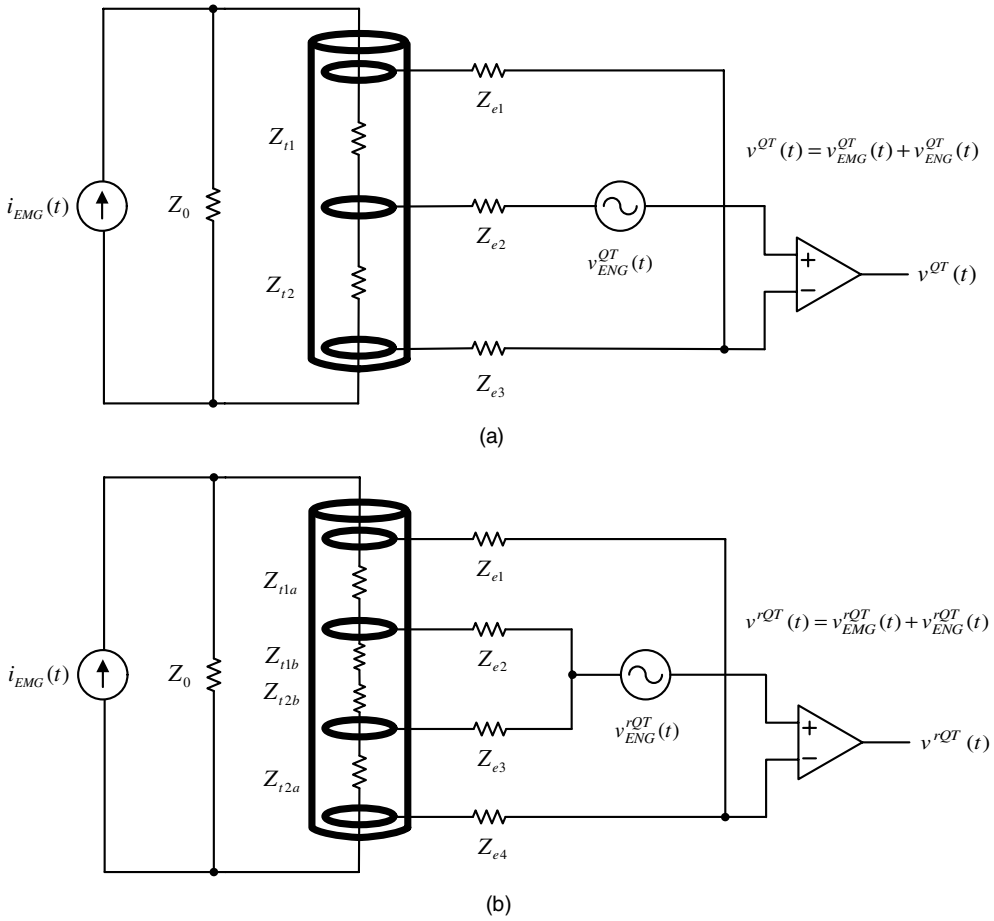

Figure 2. Lumped impedance models of (a) quasi-tripole configuration and (b) revised quasi-tripole configuration.

2. Materials and methods

2.1. Design of the nerve cuff electrode

A revised nerve cuff electrode design was proposed based on the conventional QT configuration. To clarify the advantage of the proposed design, the SIR was investigated for both the QT and rQT configurations. Figure 2(a) depicts a lumped impedance model of the QT configuration (Triantis *et al* 2008). Z_0 is the tissue impedance outside the cuff; Z_t represents the tissue impedance inside the cuff, which is separated into Z_{t1} and Z_{t2} between the middle and each end electrode; Z_{e1}, Z_{e2} and Z_{e3} are the electrode–tissue interface impedances that are assumed to be equal (i.e. $Z_{e1} = Z_{e2} = Z_{e3} = Z_e$); $i_{\mathrm{EMG}}(t)$ is the interfering EMG current that flows inside and outside the cuff, and $v^{\mathrm{QT}}_{\mathrm{ENG}}(t)$ is the ENG voltage measured at the middle electrode. It is assumed that the EMG field is linearized within the cuff and the end effects (Triantis *et al* 2005) were ignored. A cuff imbalance occurs if $Z_{t1} \neq Z_{t2}$ due to the manufacturing tolerance of the electrode positions and tissue irregularities within the cuff.

Assuming a unity gain for the amplifier, the output of the amplifier is as follows:

$$v^{\mathrm{QT}}(t) = v^{\mathrm{QT}}_{\mathrm{EMG}}(t) + v^{\mathrm{QT}}_{\mathrm{ENG}}(t) = i_{\mathrm{EMG}}(t)\frac{Z_0 Z_e (Z_{t2} - Z_{t1})}{2Z_0 Z_e + 2Z_t Z_e + Z_t Z_0} + v^{\mathrm{QT}}_{\mathrm{ENG}}(t). \tag{1}$$

Figure 2(b) shows a lumped impedance model based on the rQT configuration, where two middle electrodes are placed at the center of the cuff and shorted to the input of the amplifier. Z_{t1} and Z_{t2} are the tissue impedances inside the cuff and separated into Z_{t1a}, Z_{t1b}, Z_{t2a} and Z_{t2b} by the two middle and two end electrodes, respectively (i.e. $Z_{t1} = Z_{t1a} + Z_{t1b}$ and $Z_{t2} = Z_{t2a} + Z_{t2b}$). It is assumed that the ratios of Z_{t1a} to Z_{t2a} and Z_{t1b} to Z_{t2b} are governed by that of Z_{t1} to Z_{t2} (i.e. $Z_{t1a}/Z_{t2a} = Z_{t1b}/Z_{t2b} = Z_{t1}/Z_{t2}$), and if the middle electrodes are spaced with a distance of Δs and the cuff is designed with a distance L between the two end electrodes, the ratio $Z_{t1b} + Z_{t2b}$ to $Z_{t1} + Z_{t2}$ is determined by that of Δs to L (i.e. $(Z_{t1b} + Z_{t2b})/(Z_{t1} + Z_{t2}) = \Delta s/L$). The electrode–tissue interface impedances are assumed to be equal (i.e. $Z_{e1} = Z_{e2} = Z_{e3} = Z_{e4} = Z_e$) and $v^{\mathrm{rQT}}_{\mathrm{ENG}}(t)$ is the ENG voltage measured at the middle electrodes. Assuming a unity gain for the amplifier, the output of the rQT configuration is as follows:

$$\begin{aligned} v^{\mathrm{rQT}}(t) &= v^{\mathrm{rQT}}_{\mathrm{EMG}}(t) + v^{\mathrm{rQT}}_{\mathrm{ENG}}(t) \\ &= i_{\mathrm{EMG}}(t)\left(\left(1 - \frac{Z_p}{Z_0} - \frac{Z_p}{2Z_e}\right)\left(Z_{t1a} + \frac{Z_e(Z_{t1b} + Z_{t2b})}{Z_{t1b} + Z_{t2b} + 2Z_e}\right) - \frac{Z_p}{2}\right) + v^{\mathrm{rQT}}_{\mathrm{ENG}}(t), \end{aligned} \tag{2}$$

where

$$\frac{1}{Z_p} = \frac{1}{Z_0} + \frac{1}{Z_{t1a} + Z_{t2a} + \frac{2Z_e(Z_{t1b}+Z_{t2b})}{(2Z_e+Z_{t1b}+Z_{t2b})}} + \frac{1}{2Z_e}.$$

Now, from equations (1) and (2), the SIRs of the QT and rQT configurations are defined as follows:

$$\mathrm{SIR}^{\mathrm{QT}} = V^{\mathrm{QT}}_{\mathrm{ENG}}/I_{\mathrm{EMG}}\frac{Z_0 Z_e (Z_{t2} - Z_{t1})}{2Z_0 Z_e + 2Z_t Z_e + Z_t Z_0}, \tag{3}$$

$$\mathrm{SIR}^{\mathrm{rQT}} = V^{\mathrm{rQT}}_{\mathrm{ENG}}/I_{\mathrm{EMG}}\left(\left(1 - \frac{Z_p}{Z_0} - \frac{Z_p}{2Z_e}\right)\left(Z_{t1a} + \frac{Z_e(Z_{t1b} + Z_{t2b})}{Z_{t1b} + Z_{t2b} + 2Z_e}\right) - \frac{Z_p}{2}\right), \tag{4}$$

where I_{EMG}, $V^{\mathrm{QT}}_{\mathrm{ENG}}$ and $V^{\mathrm{rQT}}_{\mathrm{ENG}}$ are the root mean square (RMS) amplitudes of $i_{\mathrm{EMG}}(t)$, $v^{\mathrm{QT}}_{\mathrm{ENG}}(t)$ and $v^{\mathrm{rQT}}_{\mathrm{ENG}}(t)$, respectively.

As shown in equations (3) and (4), the SIRs are determined by the ENG and EMG amplitudes, which depend on the geometric parameters of the cuff electrode, such as L and Δs. Thus, to complete the expression for the SIRs, the ENG amplitude of the rQT configuration is derived for the distance Δs between the two middle electrodes. In previous studies (Struijk 1997, Andreasen and Struijk 2002), the ENG amplitude of the QT configuration was investigated for the length of the cuff L by modeling a myelinated nerve fiber as point current sources located at the nodes of Ranvier. Based on this concept, a single fiber action potential (SFAP) recorded by the *revised quasi-tripolar* cuff is described as follows:

$$\mathrm{SFAP}(t) = \sum_{k=1}^{\text{number of nodes}} i_{\mathrm{AC}}(t - kt_d) \cdot T(x_k), \tag{5}$$

where $i_{\mathrm{AC}}(t - kt_d)$ is the action current at time t and node k, and t_d is the time delay between the adjacent nodes, and $T(x_k)$ is the transfer function from node position x_k to the cuff electrode and can be interpreted as the voltage measured by the cuff electrode divided by its source current at node k. By adopting the experimental setup reported in Andreasen *et al* (2000), an example of a measured transfer function for a *revised quasi-tripolar* cuff is shown in figure 3. The transfer function can be approximated as a trapezoidal shape. According to the relationship

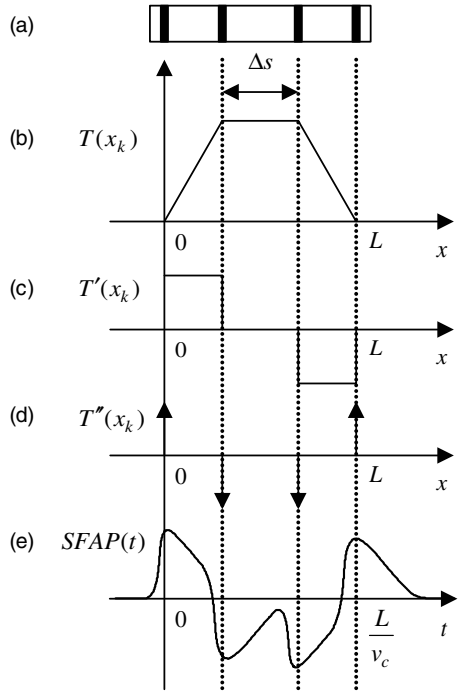

Figure 3. (a) Revised quasi-tripolar cuff, (b) measured transfer function, (c) first derivative of transfer function, (d) second derivative of transfer function and (e) single fiber action potential.

between the action current $i_{\mathrm{AC}}(t)$ and the transmembrane action potential $v_{\mathrm{AC}}(t)$, the SFAP can be rewritten as follows:

$$\mathrm{SFAP}(t) = \frac{1}{R_i}\left(v_{\mathrm{AC}}(t)T''(0) - v_{\mathrm{AC}}\left(t - \frac{L-\Delta s}{2v_c}\right)T''\left(\frac{L-\Delta s}{2}\right) - v_{\mathrm{AC}}\left(t - \frac{L+\Delta s}{2v_c}\right)T''\left(\frac{L+\Delta s}{2}\right) + v_{\mathrm{AC}}\left(t - \frac{L}{v_c}\right)T''(L)\right), \tag{6}$$

where R_i is the intra-axonal impedance per unit length within the cuff, and $T''(x)$ is the second derivative of the transfer function and related to the extracellular impedance per unit length within the cuff R_e. It can be interpreted that the SFAP is expressed as the overlap of four scaled transmembrane action potentials (figure 3(e)). The ENG signal $v_{\mathrm{ENG}}^{\mathrm{rQT}}(t)$ is then created by superpositioning the SFAPs with a uniformly randomized time delay, and the RMS amplitude of the ENG signal recorded by the *revised quasi-tripolar* cuff is calculated as follows:

$$V_{\mathrm{ENG}}^{\mathrm{rQT}} = \sqrt{\frac{\sum_{t=1}^{T} v_{\mathrm{ENG}}^{\mathrm{rQT}\ 2}(t)}{T}}, \tag{7}$$

where T is the interval of the time window.

To demonstrate the SIR improvement of the rQT configuration, a numerical calculation was done using typical impedance values and typical parameters for the EMG and ENG sources: $Z_0 = 200\ \Omega$, $Z_e = 1.0\ \mathrm{k}\Omega$, $Z_{t1} = 1.4\ \mathrm{k}\Omega$, $Z_{t2} = 1.6\ \mathrm{k}\Omega$ and $I_{\mathrm{EMG}} = 1\ \mu\mathrm{A}$ (Rahal *et al* 2000). The SFAPs and ENG signals were simulated for a 10 μm diameter fiber and 100 ms time window including 3000 SFAPs. To measure the transfer functions, silicone cuffs were made in the rQT configuration as tubes with perfect sealing and four inner Pt electrodes 1 mm wide. The inner and outer diameters were 2 mm and 4 mm, respectively. It is well known

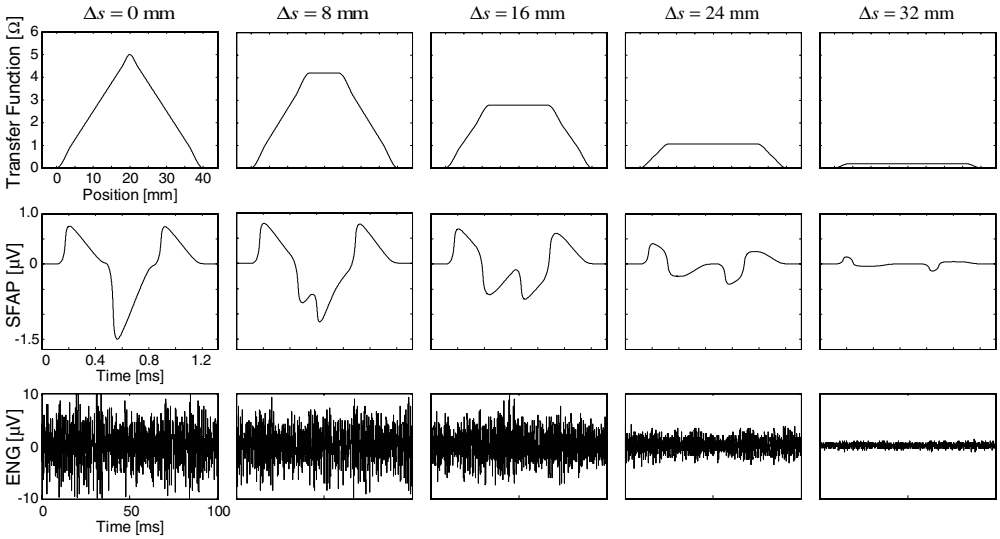

Figure 4. Examples of measured transfer functions and simulated SFAPs and ENG signals according to distance Δs.

that the ENG amplitude depends on the cuff length. To obtain the maximal signal amplitudes, the cuff length should approximate the wavelength λ of the action potentials determined by the largest fibers within the nerve bundle. Meanwhile, the wavelength of the action potential can be calculated by multiplying the duration of the spike by the conduction velocity. In the case of a 10 μm diameter fiber, the duration is about 0.67 ms and the conduction velocity is about 55.6 m s^{-1} (Struijk 1997). Therefore, the cuff length was set to 40 mm and the distance Δs between the two middle electrodes was varied from 0 to 32 mm at increments of 2 mm.

For a distance Δs of 0, 8, 16, 24 and 32 mm, examples of the measured transfer functions and simulated SFAPs and ENG signals are shown in figure 4. It is worth noting that the ENG amplitude of the QT configuration was equal to that of the rQT configuration when Δs was set to zero. In this case, the peak value of the transfer function was about 5Ω and the shape of the SFAP was generated from three transmembrane action potentials. These data are in accordance with the results when the transfer function was formulated by $T\,(L/2) = R_e L/4$ (Andreasen and Struijk 2002) and a 10 μm diameter fiber was modeled with $R_e = 500\ \Omega$ and $R_i = 30$ MΩ (Fang and Mortimer 1991). In other cases, the height of the trapezoid of the transfer function nonlinearly decreased when increasing the distance Δs thereby, affecting the amplitudes of the SFAPs and ENG signals. The influence of the distance Δs on the amplitude of the ENG signal is quantified in figure 5(a), where the curve of the amplitude was the average of 20 curves calculated with different randomized time delays for superpositioning of the SFAPs. The ENG amplitude slowly decreased for a small Δs, while it started to decrease rapidly with an increasing Δs. Meanwhile, the interfering EMG amplitude almost linearly decreased when increasing the distance Δs shown in figure 5(b). According to the definition in equation (4), the curve of the SIR was calculated, as shown in figure 5(c), which presents a concave shape with the maximum value. This means that, when compared to the QT configuration, an improved SIR can be achieved at the optimal distance Δs^* with the rQT configuration. As a result, the SIRs of the QT and rQT configurations are obtained as follows:

$$\mathrm{SIR}^{\mathrm{QT}} = \frac{V_{ENG}^{QT}}{V_{EMG}^{QT}} = \frac{3.450\ \mu\mathrm{V}}{5.714\ \mu\mathrm{V}} = 0.6038 \quad \text{at} \quad \Delta s = 0\ \text{mm}, \tag{8}$$

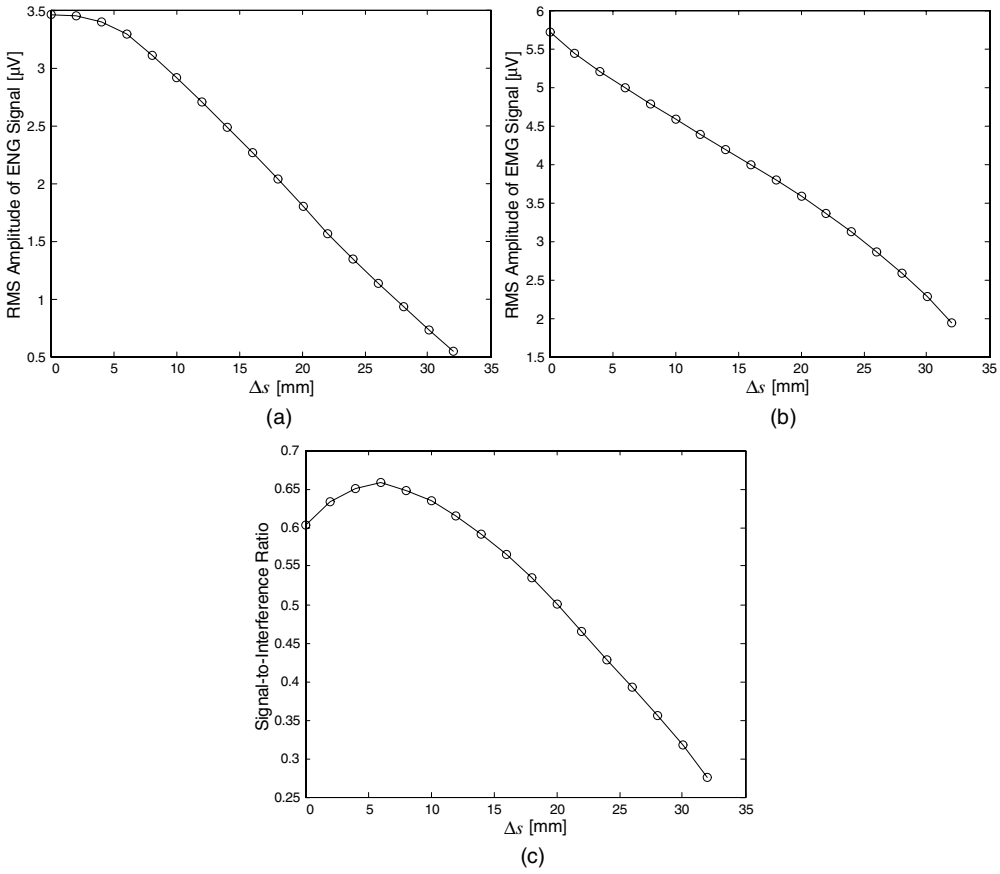

Figure 5. Influence of distance Δs on (a) amplitude of ENG signal, (b) amplitude of EMG signal and (c) signal-to-interference ratio.

$$\mathrm{SIR}^{\mathrm{rQT}} = \frac{V_{\mathrm{ENG}}^{\mathrm{rQT}}}{V_{\mathrm{EMG}}^{\mathrm{rQT}}} = \frac{3.281\ \mu\mathrm{V}}{4.987\ \mu\mathrm{V}} = 0.6580 \quad \text{at} \quad \Delta s^{*} = 6\ \mathrm{mm}. \tag{9}$$

The rQT configuration offered a better SIR in comparison to the QT configuration. Even though the recorded ENG amplitude decreased by the revision from 3.450 to 3.281 μV, the interfering EMG amplitude further decreased from 5.714 to 4.987 μV. This is because the two middle electrodes alleviate the imbalance of the tissue impedances inside the cuff.

2.2. Design of neural signal amplifier

A new neural signal amplifier design was proposed based on a preamplifier with differential passive ac coupling filters which is often encountered in different biosignal measurements and improves rejection range of differential dc input voltage (Pallas-Areny and Webster 1999, Donaldson *et al* 2003). In addition to this benefit, our ac coupled preamplifier was optimized to attain a high SNR for the purpose of application to nerve cuff electrode systems. According to noise analysis, a commercially available preamplifier and passive components were selected so that the noise floor of overall amplifier could be significantly suppressed.

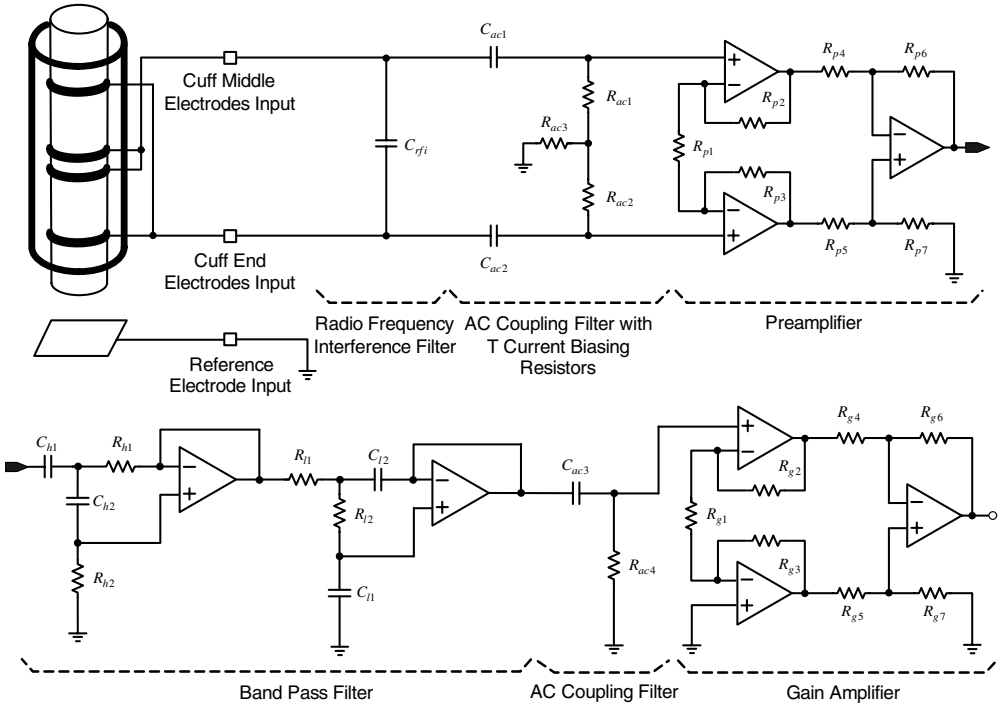

Figure 6. Block diagram of proposed amplifier.

First, the structure of the proposed amplifier is explained in figure 6 and includes a radio frequency interference (RFI) filter, ac coupling filter, preamplifier, band pass filter and gain amplifier. The ENG signal is detected by the proposed nerve cuff electrode, which is wired to the input stage of the amplifier in the rQT configuration. That is, the two end electrodes and two middle electrodes are respectively shorted and connected to the input terminals. Meanwhile, the reference electrode is located outside the cuff and grounded. The detected ENG signal is then preprocessed by the RFI and ac coupling filters before it is sent to the preamplifier. In fully implantable devices, radio frequency communication and wireless power transmission are indispensable, yet generate interference with the ENG signals. Therefore, a 1 nF capacitor C_{rfi} constitutes the RFI filter to reduce unwanted high frequencies over 60 kHz. Meanwhile, the ac coupling filter prevents a preamplifier with a high differential gain from becoming saturated due to unwanted low frequencies, such as from stimulus artifacts and EMG signals. Two 100 nF capacitors C_{ac1}, C_{ac2} and two 10 kΩ resistors R_{ac1}, R_{ac2} are used to construct a high pass filter with a corner frequency at 159.1 Hz. A 6.8 MΩ resistor is then added between the high pass filters and ground to allow a discharge path for the input bias currents. With this configuration, the two 10 kΩ resistors are large enough to detect the ENG signal without a loading effect when considering the 1 kΩ source impedance of the cuff electrode. In addition, the two 100 nF capacitors can be used to block any dc current flow through the electrodes, which can cause electrolysis or irreversible nerve damage.

Next, the preprocessed ENG signal is applied to the preamplifier. It is already known that the electronic noise of an amplifier system mostly originates from its first stage, i.e. the preamplifier. Therefore, a noise analysis was done to select a low-noise preamplifier from among several commercially available ones. Figure 7 depicts a noise equivalent model for the

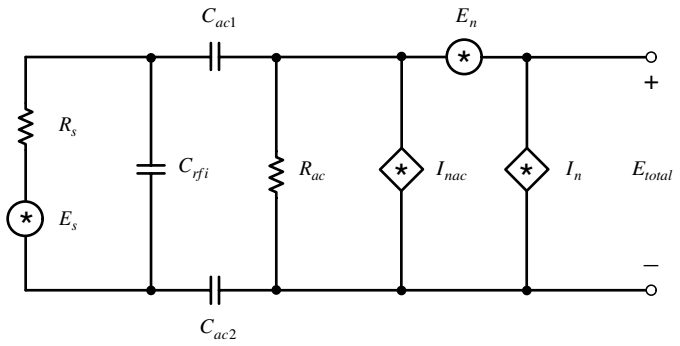

Figure 7. Noise equivalent model for cuff electrode, RFI filter, ac coupling filters, and preamplifier.

cuff electrode, RFI filter, ac coupling filters and preamplifier. The cuff electrode is described by its source impedance R_s (i.e. electrode–tissue interface impedance) and a thermal noise source $E_s = \sqrt{4\,\mathrm{k}TR_s}$, where k is the Boltzmann constant and T the absolute temperature. The ac coupling resistors R_{ac1}, R_{ac2} are expressed as a parallel resistor $R_{ac} = R_{ac1} + R_{ac2}$ and its thermal noise is represented by a current generator $I_{\mathrm{nac}} = \sqrt{4\,\mathrm{k}T/R_{ac}}$. Finally, a voltage noise generator E_n and current noise generator I_n are added for preamplification. From the noise equivalent model, the total noise E_{total} is determined consisting of the voltage noise E_v, current noise E_i and thermal noise E_{th}. Since these noises are uncorrelated, the total RMS noise can be expressed as the square root of the sum of the RMS square values of the individual noises as follows:

$$\begin{aligned} E_{\mathrm{total}} &= \sqrt{E_v^2 + E_i^2 + E_{th}^2}, \\ E_v^2 &= \int_{f_{\mathrm{min}}}^{f_{\mathrm{max}}} E_n^2 \,\mathrm{d}f, \\ E_i^2 &= \int_{f_{\mathrm{min}}}^{f_{\mathrm{max}}} I_n^2 Z_n^2 \,\mathrm{d}f, \\ E_{th}^2 &= \int_{f_{\mathrm{min}}}^{f_{\mathrm{max}}} \left(E_s^2 K_t^2 + I_{\mathrm{nac}}^2 Z_n^2\right) \mathrm{d}f, \end{aligned} \tag{10}$$

where

K_t = Transfer function from E_s to E_{total}
Z_n = Impedance between nodes of I_{nac}
f_{max} = Maximum frequency of interest
f_{min} = Minimum frequency of interest

Further computational details are given in Motchenbacher and Connelly (1993). To calculate the RMS values of these noises, some information is needed about the voltage and current noise densities for a given gain of the preamplifier, the source impedance of the cuff electrode and the frequency band of interest. In this paper, the gain of the preamplifier was set at 100, and the corresponding noise densities were used as described in the data sheets provided by the manufacturers. In addition, the source impedance was assumed to have a value of 1 kΩ, and the frequency band of interest was from 300 to 5000 Hz, where energy spectrum of the ENG signal was dominantly distributed. Table 1 lists the calculated results for the total RMS noises

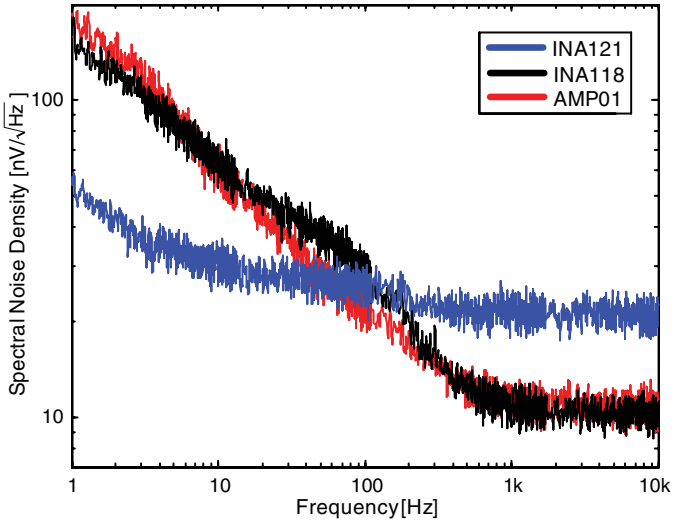

Figure 8. Spectral densities of total noises from three different amplifiers.

Table 1. Comparison of total RMS noise with various amplifiers.

	Calculated voltage noise		Calculated current noise				
Amplifier	Density nV $Hz^{-1/2}$	Noise nV	Density pA $Hz^{-1/2}$	Noise nV	Calculated thermal noise (nV)	Calculated total noise (nV)	Measured total noise (nV)
INA121	20	1371.1	0.001	0.1757	307.45	1405.2	1470.8
INA118	9	617.01	0.3	52.731	307.45	691.38	737.06
AMP01	10	685.57	0.15	26.366	307.45	751.81	783.20

of three possible commercial amplifiers. In addition, the measured results are presented, which were obtained from the spectral densities for the total noises (figure 8). These were measured on a dynamic signal analyzer (35670A, Agilent), and the difference between the calculated and measured results was caused by experimental artifacts, such as environmental noise and equipment noise floor. The INA121 (Texas Instruments) was used as the preamplifier in the neural signal amplifier developed at Cornell University (Land *et al* 2001). It was designed to record extracellular nerve signals using a needle-type microelectrode. The AMP01 (Analog Devices) is one of the best amplifiers for use with small sources. It was also adopted as the preamplifier in the nerve cuff electrode system developed at University College London (Donaldson *et al* 2003). As shown in table 1, the INA121 performed worst with the highest total noise of 1470.8 nV, while the INA118 (Texas Instruments) produced the lowest total noise of 737.06 nV. Although the INA121 had a higher input impedance and lower input bias current than the INA118 and AMP01, these characteristics did not strongly affect the performance of the preamplifier when applied to the nerve cuff electrode system, as the source impedance of the cuff electrode was small enough to prevent a large common-mode signal. Consequently, the INA118 was chosen as the preamplifier for the proposed neural signal amplifier.

One additional issue that might be of concern is the choice of the corner frequency of the ac coupling filters in terms of noise. As shown in equation (10), the current and thermal noises are related to the impedance between the nodes of I_{nac} as well as the transfer function

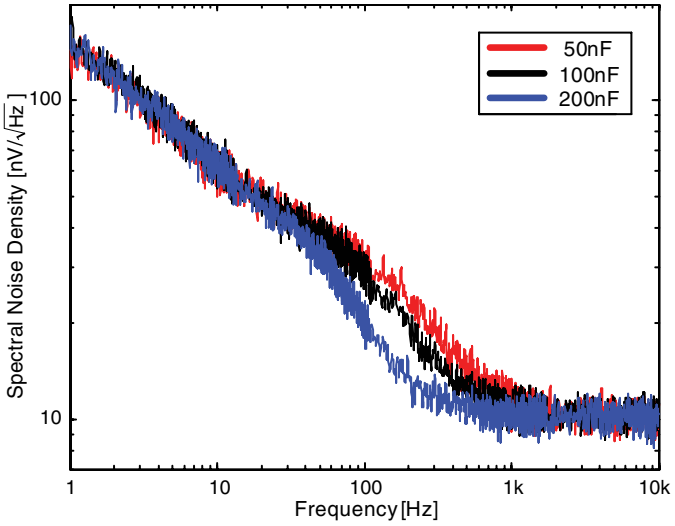

Figure 9. Spectral densities of total noises from three different capacitors for ac coupling filter.

from E_s to E_{total}, which are functions of the frequency and component value. To investigate the influence of corner frequency, noise measurement was performed for three different capacitors of the ac coupling filter (figure 9). In the case of 50 nF, the total noise measured was 766.86 nV, while the 200 nF capacitor produced a total noise of 713.53 nV. Although the 200 nF capacitor had a lower total noise than those of the 50 nF and 100 nF, a lower corner frequency of 79.5 Hz did not match the frequency band of interest from 300 to 5000 Hz, and a larger time constant of 2 ms disturbed rapid recovery from overloads due to stimulus artifacts. As a trade-off choice, the 100 nF capacitor was chosen for the ac coupling filter with a total nose of 737.06 nV.

The band pass filter and gain amplifier subsequently follow the preamplifier. The band pass filter is comprised of a second-order Butterworth high pass filter with a 300 Hz cutoff frequency in cascade with a second-order Butterworth low pass filter with a 5000 Hz cutoff frequency. The second-order Butterworth filters were implemented using a Sallen–Key topology, offering the benefits of simplicity and a non-inverting configuration. Finally, the gain amplifier is designed to have a gain of 10 and located, together with an ac coupling filter, at the output stage of the neural amplifier. To enhance the frequency response of the amplifier, an additional block is included consisting of two-stage band pass filters and a gain amplifier similar to those in the amplifier described above. As a result, the overall amplifier system has an adjustable gain from 1000 to 10 000 and a maximally flat magnitude response in a frequency range from 300 to 5000 Hz.

3. Results and discussion

3.1. In vitro experiments

3.1.1. Performance of the nerve cuff electrode. To evaluate the EMG neutralization ability of the rQT configuration *in vitro*, a saline tank experiment was performed that was modified from previous studies (Andreasen *et al* 2000, Triantis and Demosthenous 2008). As shown in figure 10, a sinusoidal signal with a 1 mA peak amplitude and 500 Hz frequency was provided

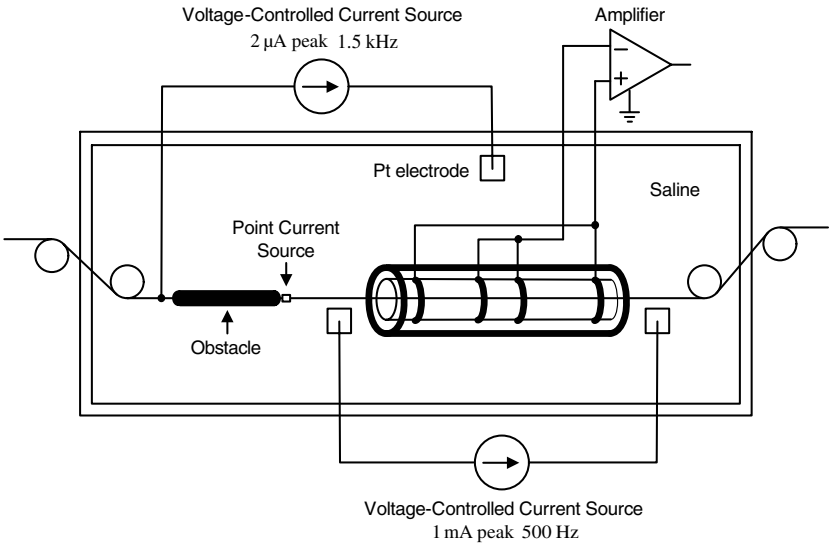

Figure 10. Saline tank experimental setup.

by a voltage-controlled current source representing the EMG current and applied to two Pt electrodes inside the saline tank. It is worth noting that the EMG signal energy spectrum is distributed dominantly from 10 to 500 Hz so that the EMG and ENG signal energy spectra overlap partially from 300 to 500 Hz. The silicone cuff made in section 2.1 was immerged in the saline (0.9% NaCl) and connected to a differential ac amplifier (A-M System, Model 1700) with a gain of 1000 and -3 dB bandwidth of 300 to 5000 Hz. To present a cuff imbalance caused by irregular tissue growth, a cylindrical-shaped obstacle (1 mm diameter and 20 mm length) was made with silicone on a Teflon-coated stainless steel wire and moved inside the cuff. The wire was stripped of insulation and the exposed portion formed a point current source (0.3 mm diameter and 0.3 mm length). Another voltage-controlled current source then provided a 2 μA peak and 1.5 kHz sinusoidal signal representing the ENG current and was connected to both the wire and the Pt electrode.

When comparing the QT and rQT configurations, two cuff electrodes with a distance Δs of 0 mm and 6 mm were used in the experiment. Figure 11(a) shows the output signal of the amplifier when the point current source was positioned at the center of the *quasi-tripolar* cuff ($\Delta s = 0$ mm). In this case, the obstacle was outside the cuff to simulate a balanced impedance. The average EMG amplitude was 0.75 mV peak, which almost coincided with the result for the *revised quasi-tripolar* cuff ($\Delta s = 6$ mm). The ENG signal was not detected visually in the time domain, yet a 1.5 kHz frequency component was observed with an amplitude of 10.4 μV peak. Next, the 20 mm long obstacle was set to occupy the left half of the 40 mm long cuff in order to assume an extreme imbalance of tissue impedance. The point current source was also positioned at the center of the cuff. The output signals for the *revised quasi-tripolar* and *quasi-tripolar* cuffs are shown in figure 11(b) and (c), and their average EMG amplitudes were 2.13 and 2.4 mV peak, respectively. In addition, the average ENG amplitudes were 9.0 μV peak for the rQT configuration and 9.3 μV peak for the QT configuration. These results indicate that, even though not perfect, the EMG field could be mostly cancelled out in the case of balanced impedance inside the cuffs. Meanwhile, when the obstacle entered the cuffs, the EMG interference was almost three times higher than that of the balanced

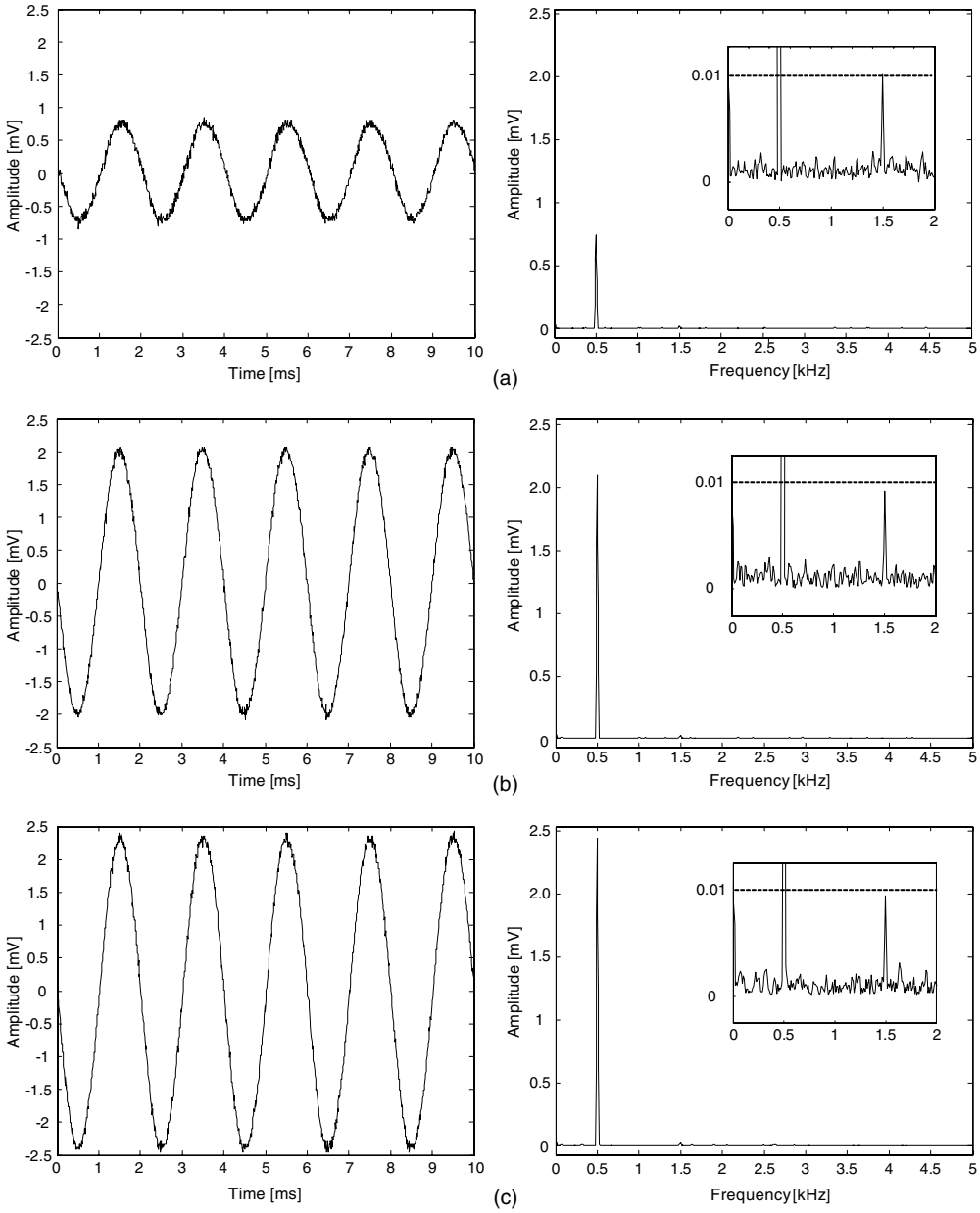

Figure 11. Output signals of (a) quasi-tripolar cuff for balanced impedance, (b) revised quasi-tripolar cuff for unbalanced impedance and (c) quasi-tripolar cuff for unbalanced impedance.

case. In this case, when compared with the QT configuration, the rQT configuration offered superior EMG neutralization, while the ENG amplitude was maintained with only a small reduction. The comparative results are summarized in table 2, where the SIRs of the rQT and QT configurations were calculated from the RMS amplitudes of the EMG and ENG signals. The SIR of the rQT configuration was about 10% higher than that of the QT configuration.

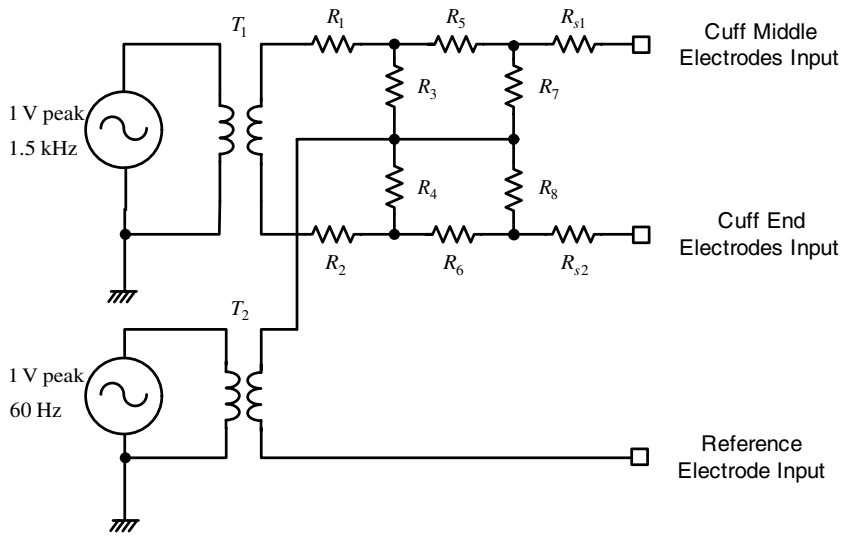

Figure 12. Evaluation circuit for generating differential and common-mode voltages.

Table 2. Comparison of signal-to-interference ratio with revised quasi-tripolar and quasi-tripolar cuffs.

	Balanced impedance condition			Unbalanced impedance condition		
Cuff	ENG (μV)	EMG (mV)	SIR	ENG (μV)	EMG (mV)	SIR
rQT	7.28	0.52	0.0140	6.36	1.50	0.004 24
QT	7.35	0.53	0.0138	6.57	1.69	0.003 88

Consequently, when a cuff imbalance was present, a higher SIR was still obtained by the proposed *revised quasi-tripolar* cuff.

3.1.2. Performance of neural signal amplifier. To investigate the performance of the proposed amplifier, the output signal and total noise were measured using an evaluation circuit, as illustrated in figure 12. Two audio transformers (NTL1, Neutrik) and a voltage divider circuit were used to simulate the differential and common-mode voltages as inputs to the amplifier. A sinusoidal signal was provided to the transformer T_1 with a 1 V peak amplitude and 1.5 kHz frequency, and attenuated by the resistors R_1–R_8 to the level of a 10 μV peak. This attenuated differential voltage represented the ENG signal and was connected to the amplifier through the 510 Ω resistors R_{s1} and R_{s2} so as to approximate the source impedance of the cuff electrode. Meanwhile, the common-mode voltage was assumed as the power-line noise. A sinusoidal signal was provided to the transformer T_2 with a 1 V peak amplitude and 60 Hz frequency, and connected to the central tap of the voltage divider without attenuation.

The improvement in SNR for the proposed amplifier was demonstrated in comparison to a differential ac amplifier (A-M System, Model 1700). First, when two function generators (AFG3022B, Tektronics) were connected to the primaries of the transformers as the differential and common-mode voltages, several cycles of the sinusoidal signal were recorded with each one of the amplifiers. Figure 13(a) shows the output signal of the proposed amplifier with a gain of 39 601 and −3 dB bandwidth of 300 to 5000 Hz, where the average amplitude

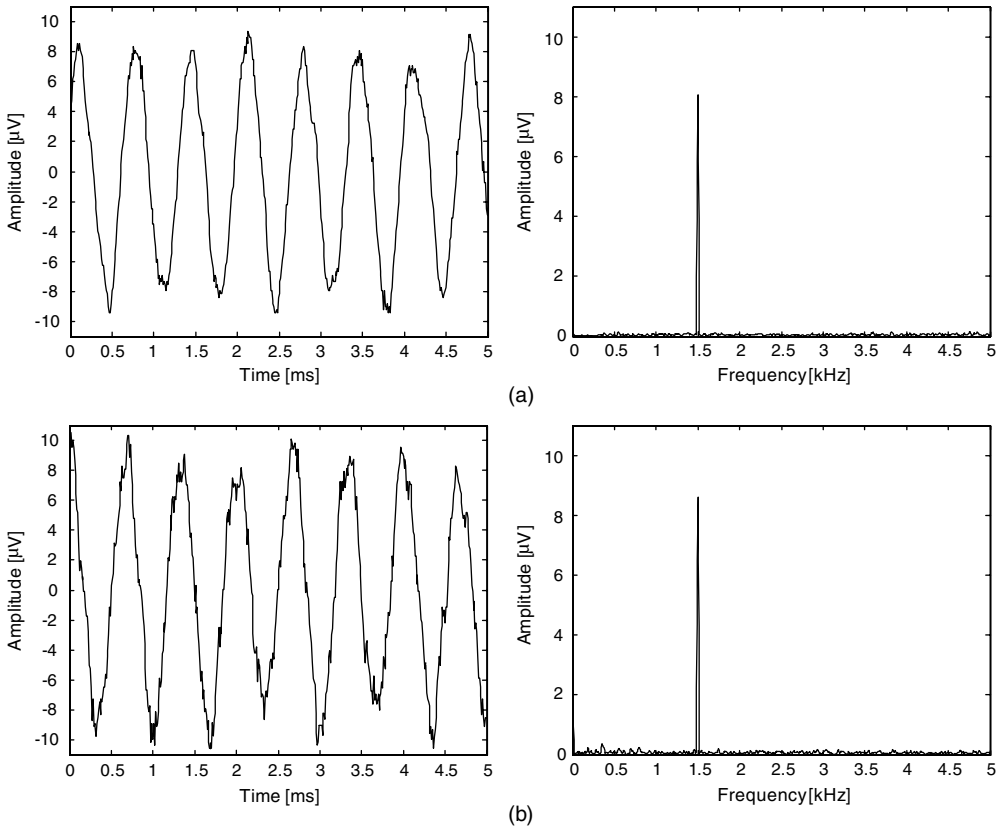

Figure 13. Output signals of (a) proposed amplifier for differential and common-mode voltages and (b) Model 1700 amplifier for differential and common-mode voltages.

was measured as a 8.124 μV peak at a frequency of 1.5 kHz. Figure 13(b) shows the output signal of the Model 1700 amplifier with a gain of 10 000 and -3 dB bandwidth of 300 to 5000 Hz, where the average amplitude was measured as a 8.599 μV peak at a frequency of 1.5 kHz. These results show that the proposed amplifier selectively filtered out the 60 Hz common-mode voltage and amplified the 10 μV differential voltage with a small noise level. However, the output signal of the Model 1700 amplifier was noisier than that of the proposed amplifier and more noise components were observed in the frequency domain. It should be noted that the amplitude of the output signals was smaller with the proposed amplifier because the ac coupling resistors in parallel to the cuff electrode attenuated the source signal. Next, to measure the total noise with only a 1 kΩ source resistor, the two function generators were disconnected from the transformers and the output signal was recorded with each one of the amplifiers. Figure 14(a) shows the time-domain and frequency-domain outputs of the proposed amplifier, where the total noise was measured as 748.39 nV for a frequency bandwidth of 300 to 5000 Hz. This value was similar to the total noise of the cuff electrode, RFI filter, ac coupling filters, and INA 118 preamplifier at 737.06 nV, listed in table 1. Thus, most of the noise of the overall amplifier system was shown to come from the preamplifier stage. Figure 14(b) shows the outputs of the Model 1700 amplifier, where the total noise was measured as 910.23 nV for a frequency bandwidth of 300 to 5000 Hz. The comparative results are summarized in table 3, where the SNRs of the proposed and Model 1700 amplifiers were calculated from the

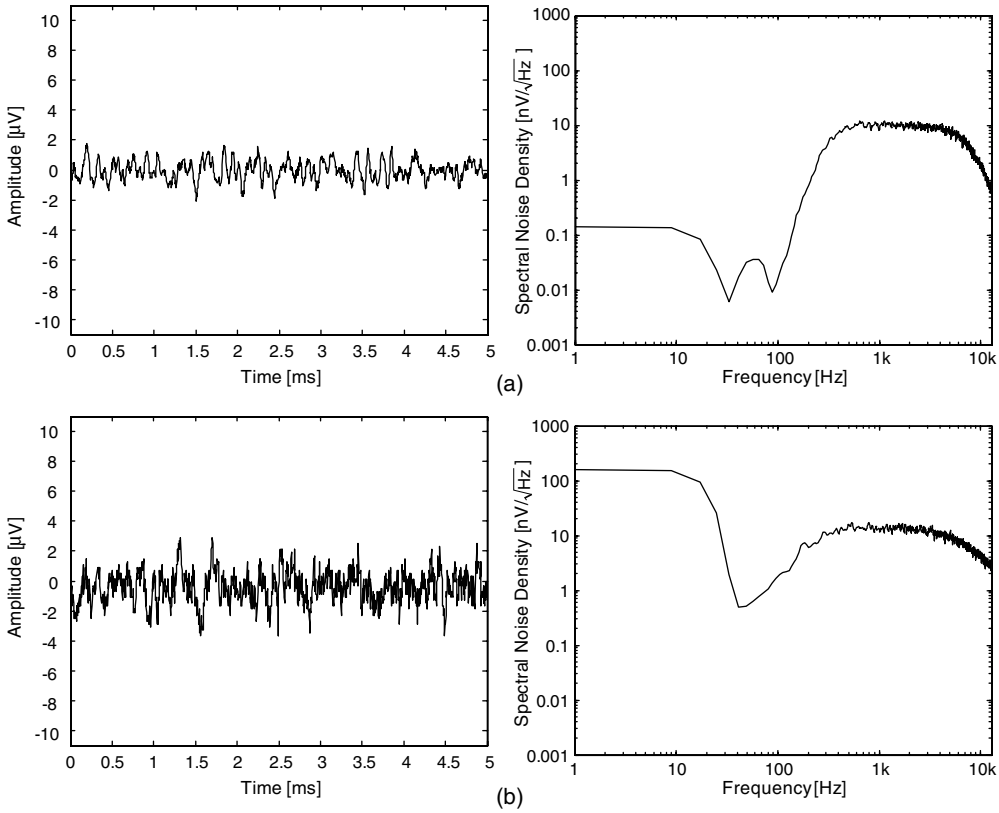

Figure 14. Output signals of (a) proposed amplifier for source resistor only and (b) Model 1700 amplifier for source resistor only.

Table 3. Comparison of signal-to-noise ratio with proposed and Model 1700 amplifiers.

Amplifier	ENG (μV)	Total noise (nV)	SNR
Proposed	5.74	748.39	7.669
Model 1700	6.08	910.23	6.679

RMS amplitudes of the sinusoidal signals, and the total noises were integrated from 300 to 5000 Hz. The SNR of the proposed amplifier was about 15% higher than that of the Model 1700 amplifier. Consequently, when the amplitude of the ENG signal was around 10 μV peak, a higher SNR, over 17 dB, was achieved with the proposed amplifier.

3.2. In vivo experiments

3.2.1. Fabrication of the proposed nerve cuff electrode system. *In vivo* experiments were performed using a rat animal model to record the ENG signals from the sciatic nerve. Therefore, the proposed nerve cuff electrode system was modified for application to a small animal model. First, the length and diameter of the *revised quasi-tripolar* cuff were redesigned to maximize the amplitude of the recorded ENG signals. In a rat sciatic nerve, the largest fibers have a diameter of about 10 μm and their wavelength is about 30–40 mm (Rodriguez *et al* 2000).

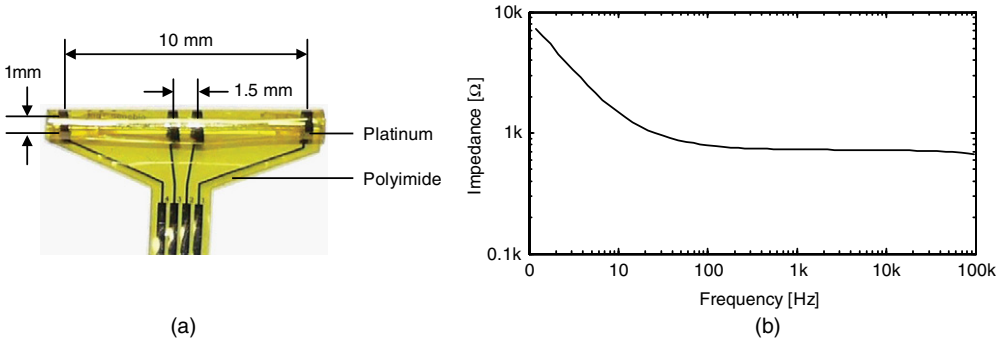

Figure 15. (a) The nerve cuff electrode and (b) impedance magnitude of the cuff electrode over frequency.

Table 4. Physical characteristics of the nerve cuff electrode.

Parameter	Measured value
Diameter	1 mm
Thickness	18μm
Distance between end electrodes	10 mm
Distance between middle electrodes	1.5 mm
Width of electrodes	0.35 mm
Impedance @ 1.5 kHz	1 kΩ

This means that a 40 mm long cuff is optimal to record the maximal signal amplitudes. However, since the length is restricted by the limited space at the implant site, the cuff needed to be trimmed to a shorter length. Nonetheless, within the anatomical constraints, the length of the cuff was extended intentionally as long as possible since even a small increase in length can increase the amplitude of the recorded ENG signals. As a result, the cuff length was 10 mm and the distance between the two middle electrodes was 1.5 mm, which were proportional to the resultant values of the numerical calculation in section 2.1. Meanwhile, the inner diameter was 1 mm so the cuff would fit the nerve tightly and prevent any damage associated with excessive mechanical stresses on the nerve. As shown in figure 15(a), the cuff electrode was constructed on a polyimide substrate with platinum electrode contacts. The polyimide substrate was self-biased to curl into a roll with an inner diameter. Moreover, a low value for the electrode–tissue interface impedance was maintained during the fabrication process to minimize the thermal noise (Lee *et al* 2010). Figure 15(b) shows the impedance magnitude of the cuff electrode over the frequency. The impedance was constantly as low as 1 kΩ in a frequency range of 300–5000 Hz. The other physical characteristics of the nerve cuff electrode are given in table 4.

Next, the proposed amplifier was implemented in such a way so that it could be divided into an implantable module and an external module. The implantable module consisted of the RFI filter, ac coupling filter, preamplifier, band pass filter and gain amplifier, while the additional two-stage band pass filters and gain amplifier were located in the external module. As shown in figure 16(a), the implantable module was then assembled together with the nerve cuff electrode, a head connector, lead wires and a hermetic case. It is already known that a parasitic capacitance exists between the lead wires connecting the cuff electrode with the preamplifier, which reduces the common-mode rejection ratio (Donaldson *et al* 2003). Thus, the cuff electrode and preamplifier were implanted together to minimize the length of

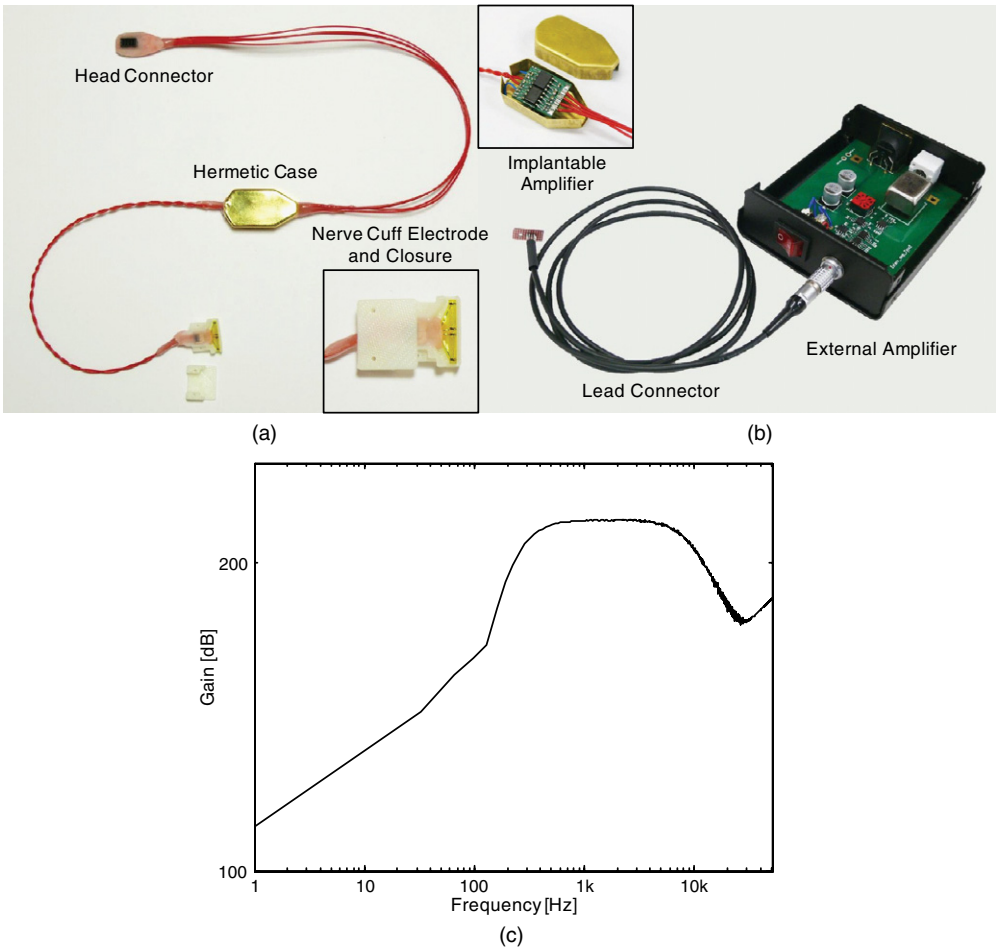

Figure 16. (a) Implantable amplifier module, (b) external amplifier module and (c) frequency response of overall amplifier system.

the lead wires. In addition, a hermetic case was used as a reference electrode to minimize the common-mode voltage between the cuff electrode and the reference electrode. The implantable amplifier module was realized on a small printed circuit board (13 mm length and 11 mm width) using surface-mounted components and encapsulated with the hermetic case to render it waterproof. When a nerve electrode is chronically implanted, an anchoring clip is usually used to provide electrical stability for the lead wires and prevent excessive force from being transmitted to the electrode when the patient moves (Amar *et al* 2008). In the proposed system, a stable electrical connection and strain relief were accomplished by means of a closure that enveloped the cuff electrode, lead wires and nerve bundle. The closure was comprised of a base plate and slider plate of a nonconductive acrylic resin material. Figure 16(b) shows the external amplifier module with a gain selector switch which was connected to the implantable amplifier module by mating the lead connector with the head connector. To reduce any hazards from current leakage, the grounds of both the amplifier and the power line were separated by a medical power supply. In addition, a transformer was used when the final output signal was

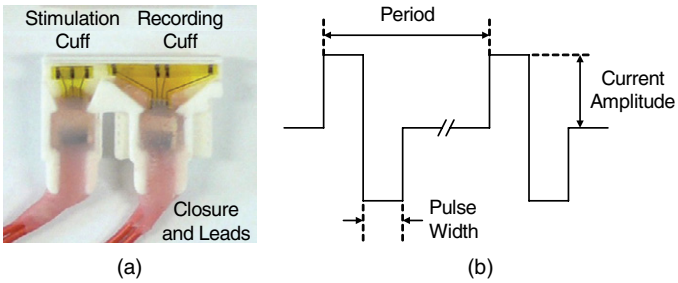

Figure 17. (a) Stimulation and recording cuffs and (b) pulse waveform for current stimulation.

Table 5. Averages of measured design parameters of proposed amplifier.

Parameter	Measured value
Minimum power supply	±2 V
Maximum power consumption	8 mW
Range of gain @ 1.5 kHz	9963–90 895
−3 dB Bandwidth @ gain 39 601	425–5500 Hz
CMRR @ 1.5 kHz, gain 39 601	115 dB
PSRR @ 1.5 kHz, gain 39 601	56 dB
Noise @1 kΩ,300–5000 Hz, gain 39 601	748.39 nV

sent to a data acquisition board. Table 5 lists the averages of the measured design parameters of the overall amplifier system. The minimum operating voltage required was ±2 V and the maximum power consumption was 8 mW. The gain could be varied in the range of 9963–90 895 at a frequency of 1.5 kHz. The frequency response was measured on a dynamic signal analyzer (35670A, Agilent), and the −3 dB bandwidth was found to be 425–5500 Hz with a gain of 39 601 (figure 16(c)). The common-mode rejection ratio and power supply rejection ratio were measured as 115 dB and 56 dB, respectively.

3.2.2. Effects of revised quasi-tripole configuration. An animal experiment was performed to show the improvement of the *revised quasi-tripolar* cuff electrode. Adult male Sprague–Dawley rats weighing 500–600 g were used for the experiments. The rats were kept and handled in accordance with the regulations of the Institutional Animal Care and Use Committee of Korea Institute of Science and Technology (KIST). During the surgical procedure for the implant placement, the rats were anesthetized with 2%–3% enflurane in O_2 through spontaneous inhalation. A skin incision was made along the thigh from the vertebral column to the knee. The biceps femoris and semitendinosus were identified and retracted to expose the sciatic nerve. After removing the surrounding tissue, the *revised quasi-tripolar* cuff electrode was wrapped around the sciatic nerve. Meanwhile, additional stimulation cuff electrode was implanted on the proximal sciatic nerve to evoke ENG signals. As shown in figure 17(a), a closure was used to fix a long-term secure position and the stimulation cuff electrode constructed on a polyimide substrate with three equally spaced ring platinum contacts. The center ring contact was used as cathode and the other two were used as anodes. The cuff length and inner diameter were set at 3 mm and 1 mm, respectively. To evaluate the effects of the rQT configuration, the SIR of the *revised quasi-tripolar* cuff electrode was compared with that of the *quasi-tripolar* cuff electrode, which was also implanted with the stimulation cuff electrode. After a healing period of one week, data recording from the sciatic nerve was

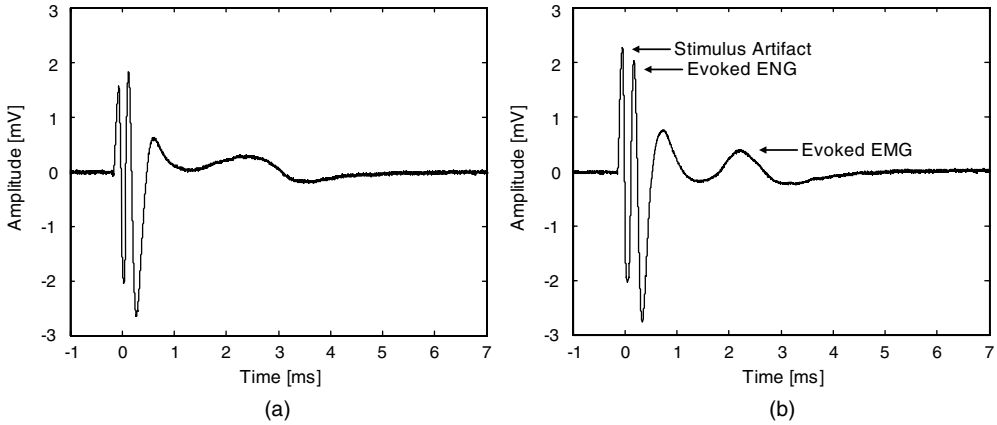

Figure 18. Stimulus artifact, evoked ENG and evoked EMG signals recorded from rat sciatic nerve during electrical stimuli with (a) revised quasi-tripolar cuff and (b) quasi-tripolar cuff.

performed with a differential ac amplifier (A-M System, Model 1700) at a gain of 1000 with a −3 dB bandwidth of 300 to 5000 Hz. The output of the amplifier was then digitized using an analog-to-digital converter board (PCI-6034E, National Instruments) with a 16-bit resolution and sampling frequency of 25 kHz. Electrical stimulation was conducted with an isolated pulse stimulator (A-M System, Model 2100), where current stimulus was a charge-balanced biphasic square pulse shown in figure 17(b). The pulse waveform had a 300 μA peak current amplitude, 100 μs pulse width and 2 s period. For each trial data were recorded for 7 ms after each stimulus pulse and each trial included ten pulses. The SIR was defined as the ratio of the peak-to-peak amplitude of the evoked ENG and either that of the evoked EMG or stimulus artifact. For each cuff electrode the average SIR was calculated from five trials and each cuff electrode was used in five rats. All the data are expressed as the mean with the standard deviation. The significance of data was determined by one-way analysis of variance (ANOVA). Values with $p < 0.05$ were considered as significantly different.

Figure 18 presents an example of the recorded stimulus artifact, evoked ENG and evoked EMG signals with an SIR close to the average. For the *revised quasi-tripolar* and *quasi-tripolar* cuffs, their average amplitudes of the stimulus artifact were 3.6104 and 4.3030 mV peak-to-peak, those of the evoked ENG were 4.4550 and 4.7213 mV peak-to-peak, and those of the evoked EMG were 0.5065 and 0.5959 mV peak-to-peak. The evoked ENG amplitude was only slightly reduced compared to the interference when the rQT configuration was applied by placing an additional middle electrode, while the internal field induced by the interference was efficiently neutralized. For the evoked EMG the average SIRs were 8.7955 $\pm$ 0.7887 for the *revised quasi-tripolar* cuff and 7.9226 $\pm$ 0.8217 for the *quasi-tripolar* cuff (figure 19(a)). The SIR of the rQT configuration was about 11% ($p = 0.026$) higher than that of the QT configuration. For the stimulus artifact the improvement in SIR was higher than for the EMG and the average SIRs were 1.2339 $\pm$ 0.1366 for the *revised quasi-tripolar* cuff and 1.0972 $\pm$ 0.1408 for the *quasi-tripolar* cuff (figure 19(b)). The SIR improved due to the rQT configuration with an increase of about 12% ($p = 0.040$) when compared to the QT configuration.

3.2.3. Effects of low-noise amplifier design. Another animal experiment was designed in such a way to demonstrate the improvement of the proposed neural signal amplifier. The

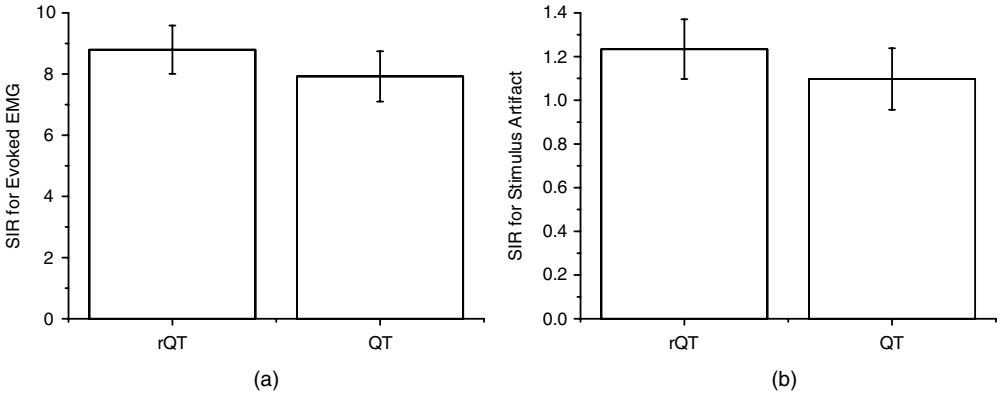

Figure 19. Signal-to-interference ratios of revised quasi-tripolar and quasi-tripolar cuffs for (a) evoked EMG and (b) stimulus artifact.

revised quasi-tripolar cuff electrode was implanted with the same procedure as described in the previous section without the stimulation cuff electrode. The implantable amplifier module was then located in a subcutaneous pocket on the back of the rats and the transcutaneous head connector was mounted on the skull. During ENG recording, the external amplifier module was connected to the implantable amplifier module by mating the lead connector with the head connector, and the gain selector was set to 39 601. To evaluate the effects of the low-noise amplifier design, the output of the proposed neural signal amplifier was compared to that of a differential ac amplifier (A-M System, Model 1700), which was directly connected to the cuff electrode with a gain of 10 000 and a -3 dB bandwidth of 300 to 5000 Hz. After a healing period of one week, the ENG signal as the final outputs of the amplifiers was then digitized using an analog-to-digital converter board (PCI-6034E, National Instruments) with a 16-bit resolution and sampling frequency of 25 kHz. The glabrous skin of the hindpaw was mechanically stimulated by von Frey filaments (Stoelting), where a 5.46 size filament was selected to apply the force from a mass of 26 g. Each mechanical stimulus continued for a duration of about 1 s and repeated about every 5 s. For each trial, the ENG signal was recorded for 50 s and each trial included ten stimuli. The SNR was defined as the ratio of the RMS amplitude of the ENG signal during the stimulus-present period and that of the noise floor during the stimulus-absent period. For each amplifier, the average SNR was calculated from five trials and each amplifier was used in five rats. Data expression and statistical analyses were performed using the same methods as described in the previous section.

Figure 20 shows an example of the recorded ENG signals with an SNR close to the average. For the proposed neural signal amplifier and Model 1700 amplifier, their average RMS amplitudes of the ENG signal during the stimulus-present period were 2.0509 μV and 2.3239 μV, respectively, and those of the noise floor during the stimulus-absent period were 0.9785 μV and 1.2914 μV, respectively. Even though the ENG amplitude decreased by the proposed low-noise amplifier design, the noise floor amplitude decreased even further. As a result, the average SNRs were 2.0959 $\pm$ 0.2315 for the proposed neural signal amplifier and 1.7995 $\pm$ 0.2681 for the Model 1700 amplifier (figure 21). These results show a higher SNR for the proposed amplifier with an improvement of 16.4% ($p = 0.016$) when compared to the Model 1700 amplifier.

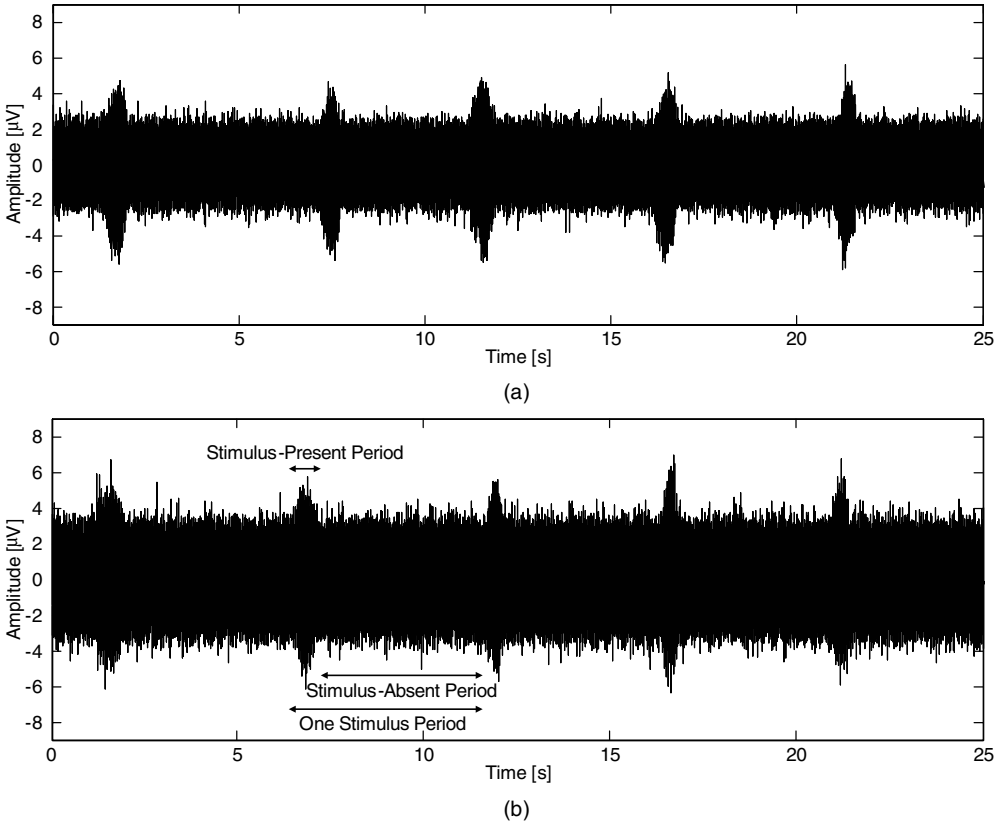

Figure 20. ENG signals recorded from rat sciatic nerve during mechanical stimuli with (a) proposed amplifier and (b) Model 1700 amplifier.

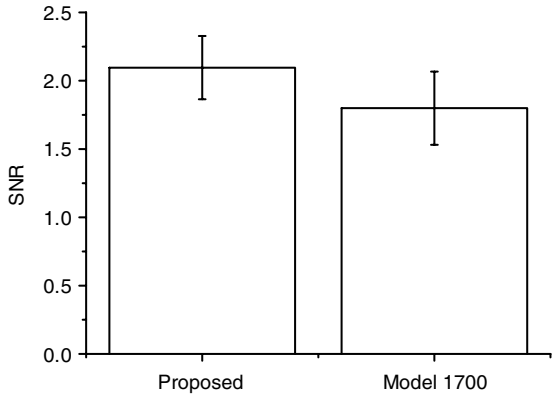

Figure 21. Signal-to-noise ratios of proposed and Model 1700 amplifiers.

4. Conclusions

This paper proposed a new nerve cuff electrode system for monitoring ENG signals from the peripheral nerves. The *revised quasi-tripolar* cuff electrode was designed to alleviate an

imbalance from tissue impedance inside the cuff. Even though the recorded ENG amplitude decreased due to the revision, the interfering EMG and stimulus artifact amplitudes decreased even further than the recorded ENG amplitude. Therefore, an improved SIR was achieved when compared to the conventional *quasi-tripolar* cuff electrode. In addition, a new neural signal amplifier design was introduced to minimize the noise generated from the preamplifier stage. The benefit of this design is that it provides a practical and low-noise preamplifier that can be easily constructed from a few commercially available components. Experimental results showed that the overall amplifier could record the ENG signals with a higher SIR and SNR. In the *in vivo* experiments, the proposed system was modified for application to a small animal model. When electrical stimuli were repeatedly presented to the animal, the interference of the stimulus artifacts and evoked EMG signals were prevented while maintaining the amplitude of the ENG signals. In addition, during mechanical stimuli, the corresponding ENG signals were measured with a large difference from the noise floor.

Although the functionality of the proposed nerve cuff electrode system was evaluated in both laboratory and *in vivo* animal tests, further safety studies for human application should be investigated to allow for clinical development. In on-going project, the proposed nerve cuff electrode system will be miniaturized to be fully implantable near a target nerve with wireless power transmission and communication modules. Moreover, it is expected that the system will also be applicable to closed loop control of FES for chronic neural recording.

Acknowledgments

This research was partially supported by the Pioneer Research Center Program through the National Research Foundation of Korea funded by the Ministry of Education, Science and Technology (20100019348), the Public welfare & Safety research program through the National Research Foundation of Korea (NRF) funded by the Ministry of Education, Science and Technology (20100020786), and the National Agenda Project funded by the Korea Research Council of Fundamental Science & Technology.

References

Amar A P, Levy M L, Liu C Y and Apuzzo M L J 2008 Vagus nerve stimulation *Proc. IEEE* **96** 1142–51

Andreasen L N S and Struijk J J 2002 Signal strength versus cuff length in nerve cuff electrode recordings *IEEE Trans. Biomed. Eng.* **49** 1045–50

Andreasen L N S, Struijk J J and Lawrence S 2000 Measurement of the performance of nerve cuff electrodes for recording *Med. Biol. Eng. Comput.* **38** 447–53

Davis L A, Gordon T, Hoffer J A, Jhamandas J and Stein R B 1978 Compound action potentials recorded from mammalian peripheral nerves following ligation or resuturing *J. Physiol.* **285** 543–59

Demosthenous A, Taylor J, Triantis I F, Rieger R and Donaldson N 2004 Design of an adaptive interference reduction system for nerve-cuff electrode recording *IEEE Trans. Circuits Syst.* **I 51** 629–39

Donaldson N, Zhou L, Perkins T A, Munih M, Haugland M and Sinkjaer T 2003 Implantable telemeter for long-term electroneurographic recordings in animals and humans *Med. Biol. Eng. Comput.* **41** 654–64

Fang Z and Mortimer J T 1991 Selective activation of small motor axons by quasitrapezoidal current pulses *IEEE Trans. Biomed. Eng.* **38** 168–74

Hansen M, Haugland M and Sinkjaer T 2004 Evaluating robustness of gait event detection based on machine learning and natural sensors *IEEE Trans. Neural Syst. Rehabil. Eng.* **12** 81–8

Hansen M, Haugland M, Sinkjaer T and Donaldson N 2002 Real time foot drop correction using machine learning and natural sensors *Neuromodulation* **5** 41–53

Haugland M and Sinkjaer T 1995 Cutaneous whole nerve recordings used for correction of footdrop in hemiplegic man *IEEE Trans. Rehabil. Eng.* **3** 307–17

Haugland M, Lickel A, Haase J and Sinkjaer T 1999 Control of FES thumb force using slip information obtained from the cutaneous electroneurogram in quadriplegic man *IEEE Trans. Rehabil. Eng.* **7** 215–27

Hoffer J A 1975 *Long-Term Peripheral Nerve Activity During Behavior in the Rabbit: The Control of Locomotion* (Ann Arbor, MI: University Microfilms)

Hoffer J A, Loeb G E, Marks W B, O'Donovan M J, Pratt C A and Sugano N 1987 Cat hindlimb motoneurons during locomotion. I. Destination, axonal conduction velocity and recruitment threshold *J. Neurophysiol.* **57** 510–29

Kurstjens G A M, Borau A, Rodríguez A, Rijkhoff N J M and Sinkjaer T 2005 Intra-operative recording of electroneurographic signals from cuff electrodes on extradural sacral roots in spinal cord injured patients *J. Urol.* **174** 1482–7

Land B R, Wyttenbach R A and Johnson B R 2001 Tools for physiology labs: an inexpensive high-performance amplifier and electrode for extracellular recording *J. Neurosci. Methods* **106** 47–55

Lee S H, Jung J H, Chae Y M, Suh J F and Kang J Y 2010 Fabrication and characterization of implantable and flexible nerve cuff electrodes with Pt, Ir and IrOx films deposited by RF sputtering *J. Micromech. Microeng.* **20** 1–8

Malagodi M S, Horch K W and Schoenberg A A 1989 An intrafascicular electrode for recording of action potentials in peripheral nerves *Ann. Biomed. Eng.* **17** 397–410

Milner T E, Dugas C, Picard N and Smith A M 1991 Cutaneous afferent activity in the median nerve during grasping in the primate *Brain Res.* **548** 228–41

Motchenbacher C D and Connelly J A 1993 *Low-Noise Electronic System Design* (Hoboken: Wiley) pp 38–52

Pallas-Areny R and Webster J G 1999 *Analog Signal Processing* (New York: Wiley) pp 104–6

Pflaum C, Riso R R and Wiesspeiner G 1996 Performance of alternative amplifier configurations for tripolar nerve-cuff recorded ENG *Conf. Proc. IEEE Eng. Med. Biol. Soc.* pp 375–6

Rahal M, Winter J, Taylor J and Donaldson N 2000 An improved configuration for the reduction of EMG in electrode cuff recordings: a theoretical approach *IEEE Trans. Biomed. Eng.* **47** 1281–4

Rodriguez F J, Ceballos D, Schuttler M, Valero A, Valderrama E, Stieglitz T and Navarro X 2000 Polyimide cuff electrodes for peripheral nerve stimulation *J. Neurosci. Methods* **98** 105–18

Sinkjaer T 2000 Integrating sensory nerve signals into neural prosthesis devices *Neuromodulation* **3** 35–41

Sinkjaer T, Haugland M and Haase J 1994 Natural neural sensing and artificial muscle control in man *Exp. Brain. Res.* **98** 542–5

Sinkjaer T, Haugland M, Inmann A, Hansen M and Nielsen K D 2003 Biopotentials as command and feedback signals in functional electrical stimulation systems *Med. Eng. Phys.* **25** 29–40

Stein R B, Charles D, Davis L, Jahamandas J, Mannard A and Nichols T R 1975 Principles underlying new methods from chronic neural recording *J. Can. Neurol. Sci.* **2** 235–44

Struijk J J 1997 The extracellular potential of a myelinated nerve fiber in an unbounded medium and in nerve cuff models *Biophys. J.* **72** 2457–69

Struijk J J and Thomsen M 1995 Tripolar nerve cuff recording: stimulus artifact, EMG, and the recorded nerve signal *Conf. Proc. IEEE Eng. Med. Biol. Soc.* pp 1105–6

Struijk J J, Thomsen M, Larsen J O and Sinkjaer T 1999 Cuff electrodes for long-term recording of natural sensory information *IEEE Eng. Med. Biol. Mag.* **18** 91–8

Triantis I F and Demosthenous A 2008 Tripolar-cuff deviation from ideal model: assessment by bioelectric field simulations and saline-bath experiments *Med. Eng. Phys.* **30** 550–62

Triantis I F, Demosthenous A and Donaldson N 2005 On cuff imbalance and tripolar ENG amplifier configurations *IEEE Trans. Biomed. Eng.* **52** 314–20